Vegetation Height Model settings and Higher Spatial Data Resolution Improve Deadwood Detection from Aerial Imagery

KATARZYNA ZIELEWSKA-BÜTTNER[1], JOHANNES KROMER[1], SELINA GANZ[2], PETRA ADLER[2] & VERONIKA BRAUNISCH[1,3]

Abstract: Large-scale mapping of standing deadwood can widely support forest management. We evaluated the effect of spatial resolution of the input data (orthophotos and Vegetation Height Models (VHMs)) and different VHM settings on the accuracy of an existing two-stage deadwood mapping approach based on random forest (RF) classification combined with an uncertainty model (UNC). The model was developed based on orthophotos of 0.5 m and a VHM of 1 m spatial resolution generated from aerial imagery of 0.2 m resolution. Higher spatial resolution of orthophotos (0.2 vs. 0.5 m) and VHM (0.5 vs. 1 m) both improved model accuracy. In addition, modifying VHM settings from the highest (VHM-H) to the lowest (VHM-L) point per pixel allowed better discrimination of deadwood from bare ground. Our results highlight the importance of thoroughly selecting spectral and structural input data settings in line with the mapping goal.

1 Introduction and motivation

Deadwood is considered an important natural forest element on which about 30 % of the forest species depend (BAUHUS & HERRMANN 2010), e.g.: bats (HENDEL et al. 2023; KORTMANN et al. 2018; Bouvet et al. 2016), saproxylic beetles (LASSAUCE et al. 2011; SEIBOLD et al. 2014) or birds (ZIELEWSKA-BÜTTNER et al. 2018; BALASSO 2016). Knowing the distribution and characteristics of deadwood is thus crucial for informed biodiversity conservation (STIGHÄLL et al. 2011; BRAUNISCH 2008; VÍTKOVÁ et al. 2018). In addition, the accumulating effects of climate-change-induced forest disturbance in Central Europe (RAKOVEC et al. 2022) have exacerbated the need for accurate deadwood information across large spatial scales. Tree dieback due to drought stress and insects' outbreaks (SCHULDT et al. 2020), especially of norway spruce (*Picea abies*) (SENF & SEIDL 2021), has dramatically changed the patterns of deadwood occurrence from small patches of targeted deadwood retention to the uncontrolled development of larger deadwood areas. Research questions regarding traffic and work safety (STEREŃCZAK et al. 2017), forest mortality (NOWAKOWSKA et al. 2020; KAMIŃSKA et al. 2020), disturbance dynamics (SENF & SEIDL 2017) and responses of forest biodiversity to disturbances (KEBRLE et al. 2022; THORN et al. 2017) have become more pressing, with serious implications for future forest management (MÜLLER et al. 2018; KUULUVAINEN et al. 2021; THOM & KEETON 2020).
In recent years, numerous remote sensing methods have been developed to map standing deadwood on various spatial scales. Studies focusing on European (SEIDL et al. 2016) or National

[1] Forest Research Institute Baden-Württemberg (FVA), Department of Forest Nature Conservation, Wonnhaldestr. 4, D-79100 Freiburg, Germany;
E-Mail: [Katarzyna.Zielewska-Buettner, Johannes.Kromer, Veronika.Braunisch]@forst.bwl.de
[2] Forest Research Institute Baden-Württemberg (FVA),
Department of Biometry and Information Sciences, Wonnhaldestr. 4, D-79100 Freiburg, Germany;
E-Mail: [Petra.Adler, Selina.Ganz]@forst.bwl.de
[3] University of Bern, Institute of Ecology and Evolution, Conservation Biology,
Baltzerstrasse 6, CH-3012 Bern, Switzerland; E-Mail: veronika.braunisch@iee.unibe.ch

(SCHIEFER et al. 2023) scales use satellite data due to their large spatial coverage, primarily Sentinel 2 data of the Copernicus Mission (ESA 2020) with a spatial resolution of 10 m. Methods utilizing higher-resolution satellite data of 1 m or higher, as provided by e.g. WorldView-3 (EUROPEAN-SPACE-IMAGING 2018), offer a viable alternative for single tree detection (LIU et al. 2021). In contrast, methods based on unmanned aerial vehicles (UAV) and aerial imagery are able to detect deadwood at the tree level (JUTRAS-PERREAULT et al. 2023; NÄSI et al. 2018), which is of great importance for some applications, such as habitat analysis for deadwood-dependent species or traffic safety operations.

Whereas flight coverage of UAV based approaches are limited to small areas, aerial imagery are suitable for applications on local and regional scales (KRZYSTEK et al. 2020). Flight campaigns and programs of the state surveys often cover entire geographical regions or states with high spatial resolution aerial imagery including red, green, blue and near-infrared (RGBI) spectral bands (ZIELEWSKA-BÜTTNER 2020), the latter being particularly advantageous for differentiating between live, declining and dead vegetation (HILDEBRANDT 1996; ZIELEWSKA-BÜTTNER 2020). Historically, aerial images were the first remote sensing data used for visual interpretation and also deadwood detection. Established protocols exist for the recognition and manual delineation of dead trees and forest areas (AFL 2003; AHRENS et al. 2004). More recently, automated deadwood detection methods were developed utilizing digital aerial imagery solely (ZIELEWSKA-BÜTTNER et al. 2020; SCHWARZ et al. 2023) or in combination with Aerial Laser Scanning (ALS) (KRZYSTEK et al. 2020; KAMIŃSKA et al. 2018; HEURICH et al. 2015). Yet, while the costs of acquiring ALS data providing valuable information on vertical tree structure still limits its operational use, aerial imagery data has been often acquired at regular intervals by state mapping agencies, their quality is continuously improving and they are increasingly accessible for free (FASSNACHT et al. 2023), making them suitable for the development of remote sensing-based monitoring.

Digital RGBI aerial imagery data bear a great potential for deadwood mapping due to its widespread availability, suitable spectral resolution and defined standards. However, similar spectral signatures of bare ground and deadwood pixels often cause a misclassification of the two (FASSNACHT 2013; ZIELEWSKA-BÜTTNER et al. 2020; MEDDENS et al. 2011). Vegetation height information is therefore an important parameter that aids identification of bare ground and low vegetation areas. VHMs based on image matching are not as accurate as VHMs from ALS (GANZ et al. 2019, WHITE et al. 2018). However, higher overlap and resolution of aerial imagery improve the quality of the VHMs (ZIELEWSKA-BÜTTNER et al. 2016) which - coupled with more detailed spectral information from higher resolution data - can facilitate more accurate deadwood detection (KAMIŃSKA et al. 2018).

In this study, we evaluated the influence of (1) an increased spatial resolution and (2) alternated resampling methods of the input data: digital orthophotos and Vegetation Height Models (VHMs) on a two-stage deadwood mapping approach based on random forest (RF) classification combined with a deadwood uncertainty model (UNC) (ZIELEWSKA-BÜTTNER et al. 2020). In addition, we tested (3) alternative VHM-settings, comparing VHMs reflecting the highest (VHM-H) or lowest (VHM-L) point per pixel, hypothesizing an improved discrimination between bare ground and deadwood with the latter approach. We focused on improvements that can be achieved using only widely available publicly acquired stereo aerial imagery data. Mapping results were evaluated for both stages (RF and UNC) to test if altered input data would improve the accuracy of the RF to an extent that would allow dropping the UNC stage of the algorithm.

2 Material and Method

2.1 Study Area

The study area of 600 ha is located around the strictly protected forest reserve “Feldseewald” of 102 ha on the northern slopes of Feldberg (1493 m a.s.l.), the highest mountain in the Black Forest (South Western Germany) (Fig. 1). In the center of the area, the mountain glacier lake “Feldsee” is located at 1100 m a.s.l. Steep slopes with bare rock formations rise from the lake to the south, west and north-west whereas the elevations to the east and north-east rise smoothly.

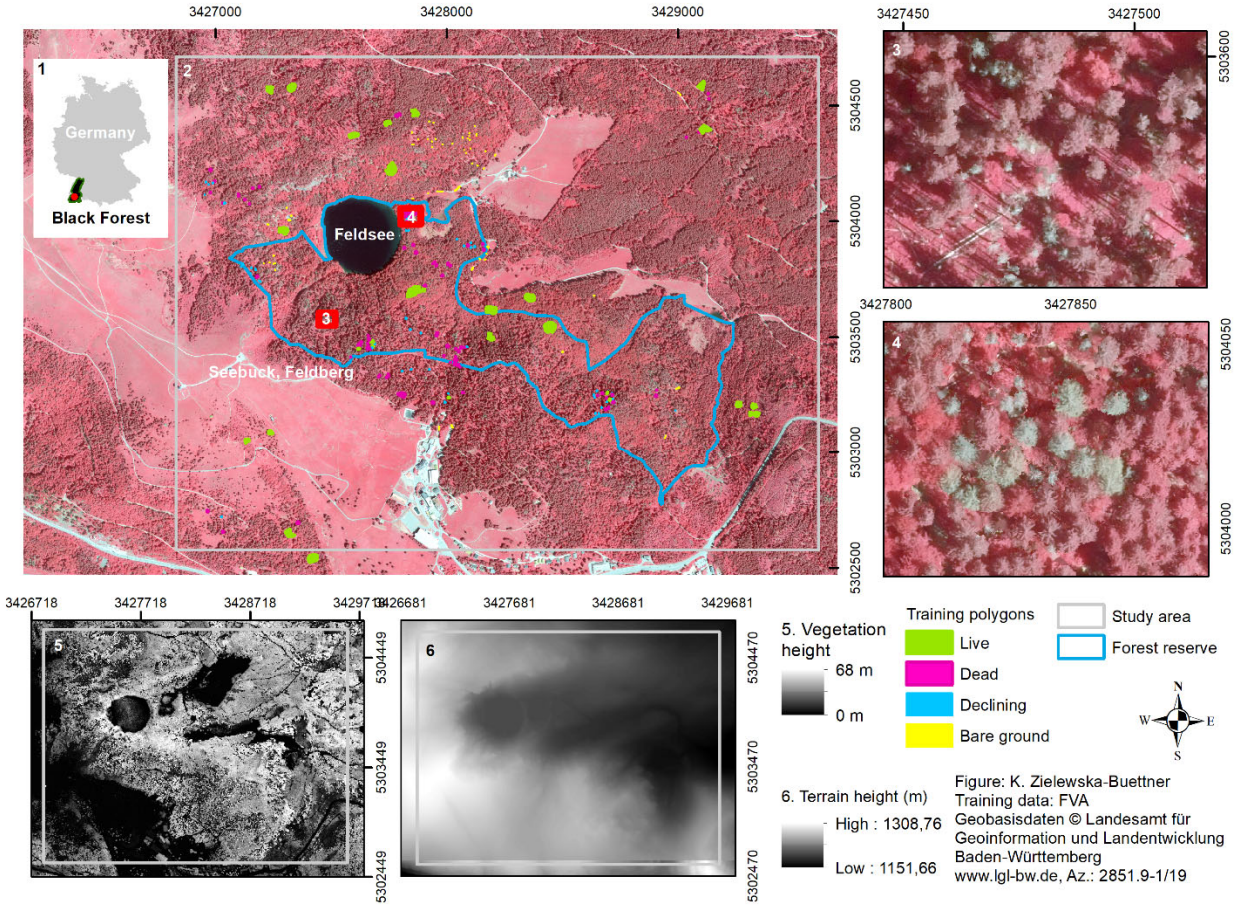

Fig. 1: Location of the study area in Germany and Black Forest region (1) with the borders of the study area, including the “Feldseewald” forest reserve, with training data polygons used for calibration of the RF models (2), examples of deadwood in the area (3, 4), Vegetation Height Model (VHM) (5), Digital Terrain Model (ALS-DTM) of the area (6). Color-infrared (CIR) orthophotos are used according to the licence agreement with the State Mapping Agency (LGL)

The unmanaged forests of the strict reserve are surrounded by large, managed forest stands with openings of mountain meadows. The montane and subalpine conifer and mixed forests is dominated by Norway spruce (Picea abies), accompanied by Silver fir (Abies alba) and European beech (Fagus sylvatica). Strict protection policy in the forest nature reserve, created in 1993, allowing natural disturbances and natural tree mortality as a part of the natural processes led to abundant retention of deadwood in different stages. Severe droughts in 2018 and 2019 (SPIECKER & KAHLE 2023), followed by bark beetle infestations, contributed to the formation of new deadwood, making the study area very suitable for studying deadwood detection and mortality.

2.2 Deadwood detection method

In this study, we evaluate the changes in input data on the performance of the deadwood detection method developed by ZIELEWSKA-BÜTTNER et al. (2020). It detects standing deadwood (h > 5 m) using orthophotos (0.5 m resolution) and VHMs (1 m resolution), derived from stereo aerial imagery of 0.5 m resolution and 60/30 % overlap (end/side lap) (Fig. 2). A two-stage algorithm classifies the input data into four model classes: bare ground, live, declining and dead trees. It includes a random forest (RF) classification followed by a "deadwood-uncertainty" filtering model (UNC), which quantifies the probability of a "deadwood"-pixel to be correctly classified as a function of the environmental and spectral conditions in its neighborhood. Before the UNC, a "slope filter" and "deep shadow mask" is applied.

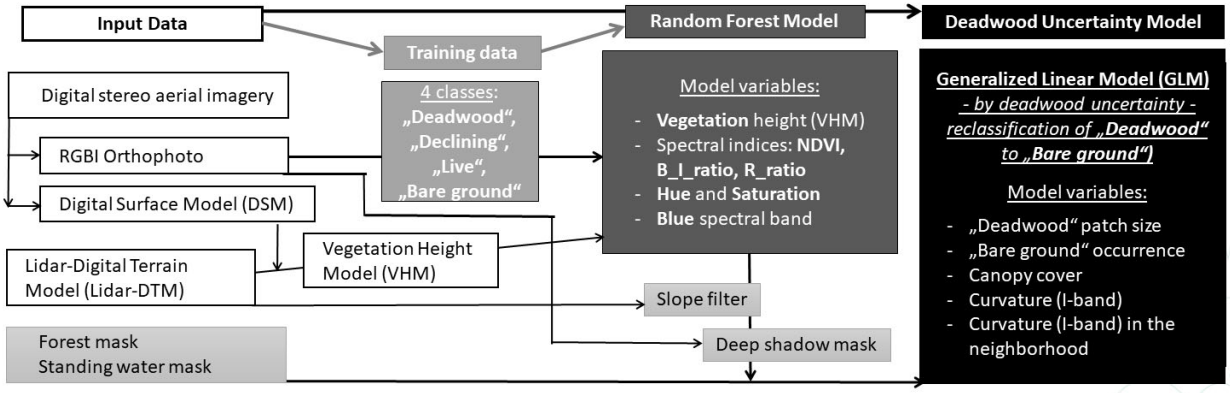

Fig. 2: Graphical representation of the workflow of the model developed by ZIELEWSKA-BÜTTNER et al. (2020) for the automated detection of standing deadwood, along with living and declining trees and bare ground. Input data, training data, as well as the predictor variables used in the random forest (RF) and deadwood uncertainty model (UNC) are illustrated in vertical sections in different shades of grey, additional filters and masks are shown in light grey boxes without frames.

2.3 Remote sensing data

The original input data for this study, including orthophotos, vegetation height model (VHM), the original aerial imagery, photogrammetric point clouds and the information on flight date and time, were provided by the state agency of spatial information and rural development of Baden-Württemberg (LGL 2022). The pan sharpened stereo aerial images contained four channels (red, green, blue and near infrared (RGBI)) with a radiometric resolution of 16 bit (Tab. 1). In line with our goal of using only publicly available data, we limited the additional data used in the study to products of LGL (Digital Terrain Model from ALS (ALS-DTM (LGL 2023b), standing water polygon layer) and internal data of the forestry administration (forest road network dataset).

The original deadwood mapping results of (ZIELEWSKA-BÜTTNER et al. 2020), which served as a reference here, were based on orthophotos of 0.5 m spatial resolution and a VHM of 1 m spatial resolution and highest point value selection per pixel. Orthophotos and VHM were derived from aerial imagery of 0.2 m resolution and 60/30 % end/side overlap generated in 2016. Between 2016 and 2019, the aerial imagery overlap changed from 60/30 % to 80/30 % end/side lap. Subsequently, the spatial resolution of orthophotos changed from 0.5 m to 0.2 m. Standard raster VHMs (LGL) retained the spatial resolution of 1 m as in 2016. However, the VHMs based on higher overlap aerial imagery data (2019) were expected to provide more accurate vegetation heights (ZIELEWSKA-BÜTTNER et al. 2016) than VHMs based on the same resolution

aerial imagery with lower overlap (2016). VHMs included the potential vegetation points of height between -1 and 55 m vs. the ALS-DTM 2000-2015.

Tab. 1: Technical characteristics of the aerial imagery data and products used for the method development (2016) (ZIELEWSKA-BÜTTNER et al. 2020) and for the comparison with data of higher resolution and overlap (2019)

Data type	Parameters	2016	2019
Aerial imagery	Camera	UltraCam Eagle	UltraCam Eagle
	Pixel size	0.2 m	0.2 m
	Overlap (end/side lap)	60/30 %	80/30 %
	Image type	Digital color infrared, RGBI	Digital color infrared, RGBI
	Flight date	08.08.2016	29.06.2019
	Flight time	07:33 - 07:39	09:25 - 09:26
	Pixel depth	16 bit	16 bit
	Coordinate System	DHDN GK3	ETRS89 UTM 32N
Orthophotos	Pixel size original data (LGL)	0.5 m	0.2 m
	Pixel size (Test)	0.5 m	0.2 m / 0.5 m
	Bands	4 (RGBI)	4 (RGBI)
Vegetation Height Model	Pixel size original data (LGL)	1 m	1 m
	Pixel size (Test)	1 m	0.5 m / 1 m
	Reference point value (LGL)	Highest (H)	Highest (H
	Reference point value (Test)	Highest (H)	Highest (H) / Lowest (L)

2.4 Tested spatial resolutions and VHM settings

Based on the data from 2019, we tested two different settings of orthophotos (with spatial resolution of 0.2 m and resampled to 0.5 m with method “bilinear” using the R package “Raster” (HIJMANS 2020). They were combined with four settings of VHMs (Fig. 3): alternative VHMs with spatial resolution of 1 m and 0.5 m were calculated, using either the highest (VHM-H) or the lowest (VHM-L) point per pixel based on the digital point clouds Digital Surface Models (DSMs) derived from the stereoscopic aerial imagery using two image matching algorithms (SCHUMACHER et al. 2019; LGL 2023a). Based on photogrammetric point clouds generated by the Software SURE (NFRAMES GMBH 2024), Digital Surface models (DSMs) were generated using a combination of lasgrid and las2tin from LASTools (RAPIDLASSO GMBH 2022). Lasgrid returned the Z-value of the highest (VHM-H) or lowest (VHM-L) point per pixel. Voids were filled with a square search radius of three pixels. Remaining voids were interpolated using the las2tin algorithm. The geometric resolution was set to 0.5 m or 1 m, respectively. To obtain vegetation heights, the difference between the DSM value and the corresponding terrain height was calculated. For this purpose, we used the raster ALS-DTM of the LGL with spatial resolution of 1 m.

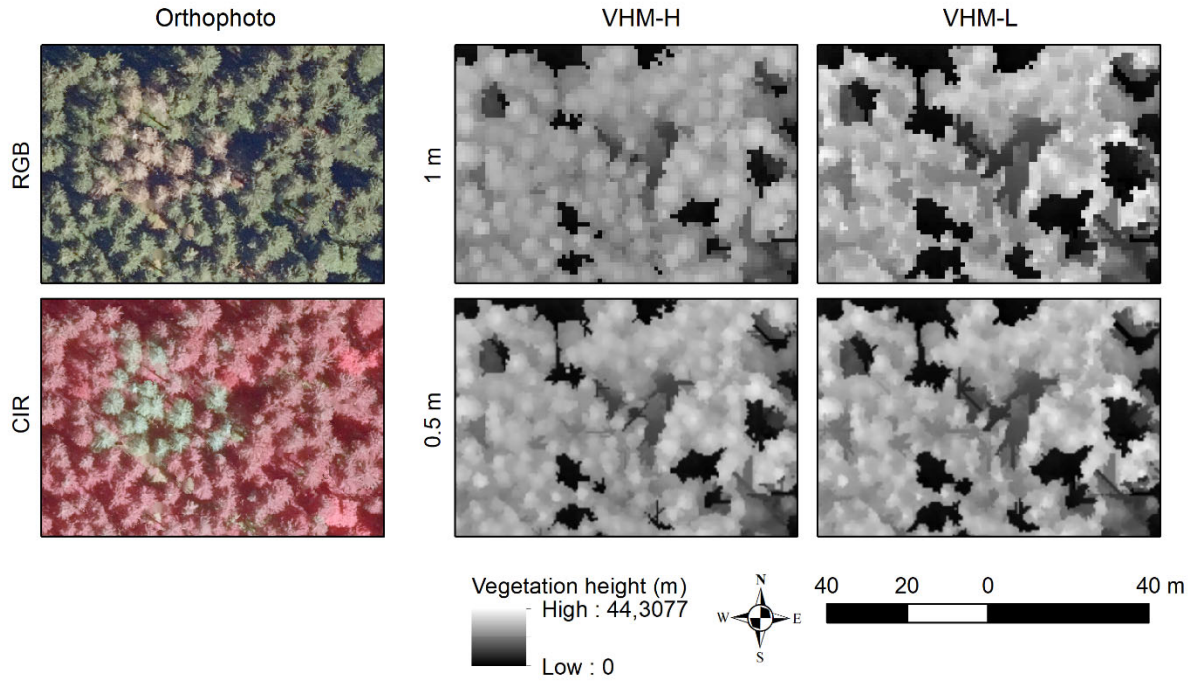

Fig. 3: Four settings of Vegetation Height Models (VHMs) characterised by different point selection value per pixel (H = highest, L = lowest) and resolution (1m or 0.5 m) with RGB and CIR orthophotos of the same area presented for a reference

Six datasets representing different combinations of spatial resolution and alternative VHMs were tested (**Fehler! Verweisquelle konnte nicht gefunden werden.**): Orthophotos of 0.2 m resolution were combined with VHMs of 1 and 0.5 m resolution as VHM-H and VHM-L, respectively. In addition orthophotos of 0.5 m resolution were combined with VHM-H and VHM-L of 0.5 m to evaluate the performance of the algorithm with the same orthophoto-resolution as in the reference model (0.5 m).

Tab. 2: Technical characteristics of the aerial imagery data and products used for method development (Reference) (ZIELEWSKA-BÜTTNER et al. 2020), for the comparison with data of higher resolution and overlap (Test) and for selection of validation pixels (Validation). The version code consists of the year – the orthophoto resolution in m (05 = 0.5 m) – the VHM resolution in m and the point per pixel selection value for vegetation height (H=highest, L=lowest)

Status	Version	Pixel size orthophoto (m)	Pixel size VHM (m)	VHM reference point
Reference	2016-05-1H	0.5	1	H
Test	2019-02-1H	0.2	1	H
Test	2019-02-1L			L
Test	2019-02-05H	0.2	0.5	H
Test	2019-02-05L			L
Test	2019-05-05H	0.5	0.5	H
Test	2019-05-05L			L
Validation	2019-02-04L	0.2	0.4	L

To compare the different VHMs (Fig. 3) with each other and to evaluate their influence on the deadwood mapping results we analyzed the distribution of vegetation heights in the test datasets. Expecting the biggest differences in the low and high forest areas, we calculated the

amount of pixels in following height classes: < 1 m, ≥ 1 m & < 2 m, ≥ 2 m & < 5 m, ≥ 5 m & < 20 m, ≥ 20 m.
As an additional, independent dataset for selecting the validation sample, we used an orthophoto of 0.2 m and a VHM-L of 0.4 m resolution.

2.5 Validation

Deadwood mapping results of all data combinations were validated based on visual interpretation of orthophotos in the corresponding resolutions of 0.2 m and 0.5 m. Two validation datasets of 0.2 m and 0.5 m were acquired based on a stratified random sampling of 500 pixels per model class drawn from the RF mapping results of an independent dataset (2019_02_04L) (**Fehler! Verweisquelle konnte nicht gefunden werden.**Tab. 2, Appendix 1). Different masking and mapping results per dataset resulted in slightly different numbers of pixels in each model class (Appendix 2,

Appendix 3). The two sets of validation pixels were visually interpreted according to the following keys: bare ground, live, declining, dead, building (construction element), orthophoto artefact and deep shadow.
For all test datasets, the mapping results of both model steps (RF and UNC model) were validated against the validation sample with the same resolution as the included orthophoto (0.2 m or 0.5 m). User's accuracy (UA), producer's accuracy (PA) and F1-score (Equation 1) for the class "deadwood" and overall accuracy (OA) and Kappa across all model classes were calculated using the package "Caret" version 6.0-94 (KUHN et al. 2023) in R- 4.2.3 (R-CORE TEAM 2023) and R-Studio (RSTUDIO 2023).

Equation 1: F1score = 2 * Precision * Recall / Precision + Recall

3 Results

3.1 Vegetation height models

By changing the settings for the rasterization of the point cloud, four different VHMs (**Fehler! Verweisquelle konnte nicht gefunden werden.**, Fig. 3) with slightly differently distributed height values were generated for the study area. The biggest differences between the VHM pixel distributions were observed for heights below 1 m and above 20 m (Fig. 4). For both tested resolutions, the point selection value resulted in more pixels with low heights (< 1 m) in the VHM-L and more pixels in the highest category (≥ 20 m) in the VHM-H. This pattern was stronger in the settings including the lower resolution VHMs (1 m). The percentage of pixels was stable for the height range from 2 m to 20 m, with variation of 1 % or less between the different VHM datasets.

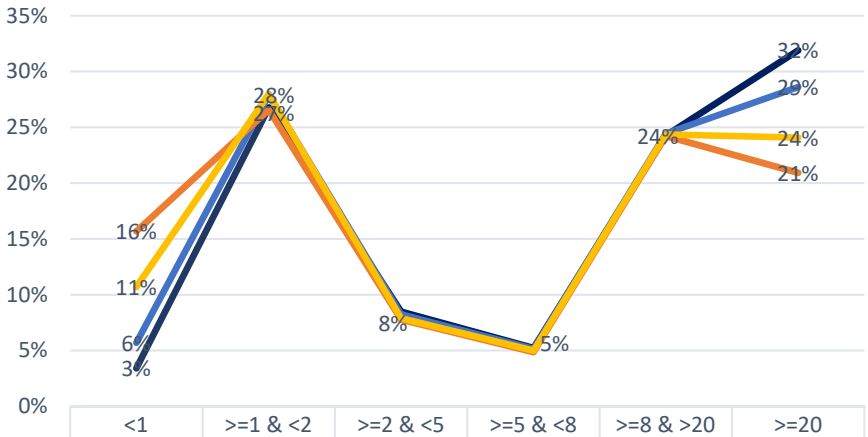

	<1	>=1 & <2	>=2 & <5	>=5 & <8	>=8 & >20	>=20
2019_02_1H	3%	27%	8%	5%	24%	32%
2019_02_05H	6%	28%	8%	5%	24%	29%
2019_02_1L	16%	27%	8%	5%	24%	21%
2019_02_05L	11%	28%	8%	5%	24%	24%

Fig. 4: Percentage of pixels in different height classes (m) obtained with different settings of the vegetation height model (VHM). VHMs with the highest point value per pixel are presented in blue and with the lowest point value per pixel in yellow-orange. Lighter colors mark higher resolution VHMs. Datasets are specified in Table 2

3.2 Mapping results

For each dataset more than half (56 – 63 %) of the study area was masked out from the further analyses (Tab. 3), i.e. as lake, meadow, low vegetation or non-forest area with a height of less than 5 m (see also Fig. 4: Percentage of pixels in different height classes (m) obtained with different settings of the vegetation height model (VHM)Fig. 4) or deep shadow. The largest area was masked out for the VHM-L settings: 2019-02-1L (63 %), 2019_02_05L and 2019_05_05L (both 60 %) and the smallest for datasets with VHM-H: 2019-02-1H (56 %), 2019-05-05H and 2019-02-02H (both 57 %). The area with heights of less than 5 m contributed most significantly to the masked areas, especially for VHM-L settings: 2019-1L (50 %) and 2019-05L (47 %), and less for VHM-H settings 2019-1H (39 %) and 2019-05H (42 %).

Tab. 3: Mapping results for the reference (2016-05_1H) and six test datasets at two stages of the mapping algorithm (Random Forest model – RF, Uncertainty model – UNC), expressed in area mapped (ha). Masked area (ha) and mapped area per model class: „bare ground“, „live“, „declining“ and „dead“ (vegetation), as well as the total study area are presented. Note that only the results for the classes „bare ground“ and „dead“ change between RF and UNC. Datasets are specified in Table 2

Dataset	Masked area (ha)	Model class area (ha)						Sum area (ha)
		Bare ground		Live	Declining	Dead		
		RF	UNC	RF = UNC		RF	UNC	
2016_05_1H	323,3	0,9	1,3	233,5	31,9	3,0	2,6	592,6
2019_02_1H	333,2	0,6	0,8	192,5	60,9	5,0	4,8	592,2
2019_02_1L	372,1	0,1	0,2	164,7	52,2	3,0	2,9	592,2
2019_02_05H	339,2	0,4	0,7	187,5	60,4	4,6	4,4	592,2
2019_02_05L	354,3	0,2	0,3	176,0	58,1	3,7	3,5	592,2
2019_05_05H	336,1	0,3	1,3	192,4	58,8	4,5	3,4	592,2
2019_05_05L	352,4	0,2	1,1	181,1	54,4	4,1	3,1	592,2

In the deadwood mapping process two outputs corresponding to two-stages of the method (RF and UNC) were generated and analyzed per test dataset. The model class “live” was the most

abundant in both mapping stages, including 32 - 33 % of the study area for datasets including VHM-H and 28 - 31 % for VHM-L datasets. The class declining was comprised 10 % of the study area for datasets with VHM-H and 9 - 10 % for VHM-L. Deadwood and bare ground pixels varied between 0 and 1 %, corresponding to 2.9 - 5 ha (deadwood) and 0.1 - 0.8 ha (bare ground).

3.3 Deadwood and pixel resolution

Focusing on the improvement of deadwood detection only the results for the class “dead” are provided here, full results are included in Appendix 2 and
Appendix 3.
In 2019 between 2.9 and 5 ha deadwood was mapped depending on the test dataset, compared to 2.6 (RF) and 3 ha (UNC) in the reference dataset from 2016 (**Fehler! Verweisquelle konnte nicht gefunden werden.**). When comparing the datasets with the same resolution, more deadwood was mapped in all datasets with VHM-H than with VHM-L (Appendix 4). In addition, the coarser VHM resolution of 1m produced the most deadwood pixels with VHM-H and the least with VHM-L of all tested datasets. In the datasets with orthophoto resolutions of 0.2 m differences between VHM-H and VHM-L pairs were larger than in the datasets orthophoto resolution of 0.5 m.

3.4 Deadwood, bare ground and the influence of the stage of the algorithm

In all test datasets with 0.2 m orthophoto-resolution the amounts of mapped pixels of the classes “deadwood” and “bare ground” did not differ much between the RF and UNC model stages (Tab. 3). In contrast, the model class changes from “dead” to “bare ground” after UNC model application was very pronounced in the datasets with 0.5 m resolution (Appendix 4). Regardless of the model stage less than 1ha bare ground was mapped for test datasets with 0.2 m resolution. For test datasets with 0.5 m resolution bare ground amounts increased significantly between RF and UNC from 0.2 - 0.3 ha to 1.1 and 1.3 ha. In the reference dataset the model class change was also distinct, although not as pronounced as for test datasets.

3.5 Model performance

Input data with higher resolution (2019) delivered in all cases more accurate mapping results than the lower resolution baseline data (2016) (Tab. 4). OA increased from 0.70 (RF) and 0.74 (UNC) in 2016 to in average 0.79 in 2019. Similarly, Kappa values increased from 0.60 (RF) and 0.65 (UNC) to in average 0.72. The best OA and Kappa values were calculated for both RF and UNC based on the 2019-05-05L dataset (OA = 0.80 and 0.82 and Kappa = 0.74 and 0.75, respectively) with the second-best dataset being 2019-02-05L resulting in similar OA of 0.80 and slightly lower Kappa values of 0.73 and 0.72 for RF and UNC, respectively. The worst, but still outperforming the 2016 results were obtained with the 2019-05-05H dataset, with OA = 0.76 and Kappa = 0.69 (RF) and OA = 0.78 and Kappa = 0.71 (UNC). For both RF and UNC, models based on datasets incorporating VHM-Ls always performed better than the corresponding models using standard VHM-Hs.
Two-stage deadwood mapping with UNC provided almost always equally good or better results than stand-alone RF models, with the most significant increase in mapping accuracy observed for the datasets including an orthophoto of 0.5 m resolution. Only the Kappa value for the RF results of 2019-02-05L was higher than for the second stage of the algorithm.

Tab. 4: Validation results of the two stage-deadwood mapping model (ZIELEWSKA-BÜTTNER et al. 2020) applied to different datasets. Evaluation metrics are provided for both stages of the algorithm (Random Forest and Uncertainty Model), with UA = user's accuracy, PA = producer's accuracy and F1-score indicating the accuracy to predict the model class „deadwood" and OA = overall accuracy and Kappa value quantifying overall model performance. The best results are marked in bold. Datasets are specified in Table 2.

Dataset	Ortho_ VHM resolution	VHM settings	Random Forest Model					Uncertainty Model				
			Deadwood			Model		Deadwood			Model	
			UA	PA	F1-score	OA	Kappa	UA	PA	F1-score	OA	Kappa
2016-05-1H	05_1	H	0.60	0.82	0.69	0.70	0.60	0.74	0.80	0.77	0.74	0.65
2019-02-1H	02_1	H	0.71	0.88	0.78	0.79	0.72	0.71	0.87	0.79	0.79	0.72
2019-02-1L		L	0.74	0.84	0.79	0.79	0.72	0.74	0.84	0.80	0.79	0.72
2019-02-05H	02_05	H	0.73	0.88	0.80	0.79	0.72	0.75	0.88	0.79	0.79	0.72
2019-02-05L		L	**0.75**	0.87	**0.81**	**0.80**	0.73	0.77	0.84	0.81	0.80	0.72
2019-05-05H	05_05	H	0.68	0.91	0.78	0.76	0.69	0.79	0.86	0.84	0.78	0.71
2019-05-05L		L	0.72	**0.89**	0.80	**0.80**	**0.74**	**0.82**	**0.89**	**0.85**	**0.82**	**0.75**

3.6 Deadwood mapping

Greater differences than for overall model accuracy were observed for the mapping results for the deadwood class. The best RF results were obtained with the highest tested resolution VHM-L (2019-02-05L), with UA = 0.75, PA = 0.87 and F1-score = 0.81followed by VHM-L (2019-05-05L) with deadwood UA = 0.72, PA = 0.89 and F1-score of 0.80. This data combination provided also the best overall result for the UNC model with UA = 0.82, PA = 0.89 and F1-score = 0.85. All models by far outperformed the results of the reference dataset, for both RF: UA = 0.60, PA = 0.82, F1-score = 0.69 and the UNC: UA = 0.74, PA = 0.80, F1-score = 0.77. With a VHM resolution of 0.5 m, RF models alone always provided equal or higher PA values than in combination with UNC while with VHM of 1m PA and UA values remained the same.

4 Discussion

Validation results confirm that both the resolution of orthophotos and VHMs as well as the VHM point selection method (lowest or highest point per pixel) affected the mapping results. In all cases, models based on the higher-resolution data from 2019 outperformed the results based on the reference dataset of 2016 in deadwood mapping accuracy and overall model performance.

Different amounts of deadwood were mapped across algorithm stages, datasets and acquisition years. While visual inspection of the orthophotos confirmed an increase in deadwood between 2016 and 2019, reflecting the tree damages and bark beetle infestations during the drought years of 2018 and 2019 (SPIECKER & KAHLE 2023), different deadwood amounts mapped in the same year across different datasets highlight the multifaceted influences impacting deadwood mapping accuracy.

4.1 Influence of spatial resolution

Deadwood mapping accuracy and overall model performance increased, as expected, with spatial resolution, as confirmed for resolutions between 0.5 and 5 m by PLUTO-KOSSAKOWSKA et al. (2017).

The most pronounced influence of the spatial resolution only (while using VHM-H) was evident for the RF results, where the accuracy measures improved with all datasets by 0.8 – 0.13 in

comparison to the results of 2016 (Table 4). The highest accuracies for RF delivered datasets with the highest tested resolution of orthophoto and VHM (2019-02-05).
The smallest increase in model accuracy was observed for the datasets including VHMs with the coarser resolution of 1 m. Here the smoothing effect on the vegetation heights was probably the cause of inaccuracies in areas with low vegetation, followed by misclassifications of bare ground as deadwood (ZIELEWSKA-BÜTTNER et al. 2020). However, the high resolution of the orthophoto in 2019 (0.2 m) still contributed to raising the model results to an acceptable level.
The UNC model improved at most the classification results for the datasets with 0.5 m resolution, with the best combination being 2019-05-05L. The reason is most likely an exact match in resolution between the test datasets and the settings of the fixed UNC model, that was developed based on orthophotos and RF results of 0.5 m resolution.

4.2 Influence of vegetation height model settings

The point selection value for the VHM contributed further to improving the RF mapping accuracies, especially regarding the UA of the deadwood class, which is crucial for the map user, as too large commission errors can lead to meaningless field campaigns and ineffective use of resources (FASSNACHT et al. 2014). VHMs with the lowest point value selected per pixel delivered higher accuracies than the initial settings using the highest point per pixel. Low point selection in the VHMs led to a more accurate identification of low forest height areas, thereby reducing the misclassification of bare ground as deadwood. However, it also contributed to masking out larger areas by cutting off more pixels on forest and tree edges. Consequently, a smaller deadwood area was mapped using VHM-L, but the advantage of an accurate mapping prevailed over a disadvantage of possible underestimation of deadwood area. Differences between the VHM settings were most pronounced in the height classes < 1 m and ≥ 20 m, with the greatest deviations in areas where both classes meet, e.g. at the tree outer parts, at stand borders along forest edges, roads and gaps.

4.3 Mapping accuracy

The second-stage of deadwood mapping with UNC improved the overall model performance only for datasets with resolutions of 0.5 m. For the accuracy of mapping the class deadwood, the influence of UNC was more pronounced and its application improved the UA and F1 score for almost all datasets including an orthophoto of 0.5 m resolution. The increase in UA usually came with the cost of a slight decrease in PA, however not below 0.84 (2019-02-05L), which can still be considered as very good.
Deadwood mapping accuracies (PA of 0.84 - 0.91) achieved with all test datasets are comparable with those obtained by KAMIŃSKA et al. (2018) (PA for dead spruce of 0.76 – 0.90) based on color-infrared (CIR) aerial imagery and VHM from ALS, who, however, used only well visible dead trees for validation. VHMs from ALS are known to be more detailed and accurate than the VHMs from image matching of stereo aerial imagery (GANZ et al. 2019; WHITE et al. 2018; WHITE et al. 2016), on which our models were based on. KRZYSTEK et al. (2020) mapped standing dead trees with an UA of 0.93 – 1 and PA of 0.93 – 1 (based on a test reference dataset and depending on the study site) using ALS with a point density of 55 pts/m² and multispectral aerial imagery of spatial resolution of 0.17 m. The detection of snags was less successful with an UA = 0.56 and PA = 0.66.
In all our tests, F1-scores ranged between 0.78 and 0.85. These results are comparable to those of other authors using data of similar spatial resolution with other methods. HELL et al. (2022) reported F1-scores of 0.78 and 0.77 while using a PointCNN algorithm for the classification of

snags and dead trees with ALS point clouds (max. point density of 80 pts/m²) and CIR true orthophotos (0.2 m resolution). LIU et al. (2021) achieved for standing deadwood class a F1-score = 0.93 using a novel Pixel- and Object-based Image Fusion Method incorporating different mapping algorithms with the WorldView3 data of 0.5 m resolution. We identified only one method for large-scale deadwood mapping based solely on aerial imagery products developed by SCHWARZ et al. (2023). The authors mapped conifer canopy mortality based on a deep learning approach using aerial images across Luxembourg with a F1-score of 0.725 – 0.759. Our results corresponding to these based on ALS data or other models indicate further potential in the exploration of the image based VHMs in line with the different mapping purposes.

4.4 Conclusions

Our study proves that accurate, large-scale area-wide mapping of standing deadwood is possible using solely orthophotos and VHM from image matching of stereo aerial imagery. The choice of the best dataset, however, may depend on the mapping targets. In this context, time and processing resources as well as large data storage requirements are important factors to consider. Comparing different datasets, 2019-05-05L UNC provided the best results. Although additional data processing was needed for the UNC, data preparation and processing time for the two-step procedure with a data resolution of 0.5 m was considerably shorter than for a standalone RF model with a resolution of 0.2 m (2019-02-05L), which would be the second-best choice, because of the lower UA and the longer processing time. For large-scale deadwood mapping we consider the resolution of 0.5 m sufficient. Even if some thin snags might not be captured, they usually represent only a very small share of the overall deadwood, and the area they cover is neglectable when data is aggregated. In older disturbance areas, however, with large aggregations of deadwood in high decay stages, deadwood amounts might be seriously underestimated. For small-scale analyses, an intermediate RF data with a higher PA and visual control may thus be preferable.

5 Acknowledgements

The study was carried out at the Forest Research Institute Baden-Württemberg (FVA) with the data contribution of the State Agency of Spatial Information and Rural Development of Baden-Württemberg (“Geobasisdaten ©LGL, Landesamt für Geoinformation und Landentwicklung Baden-Württemberg, www.lgl-bw.de, AZ.:2851.9-1/19.)

6 References

AFL ARBEITSGRUPPE FORSTLICHER LUFTBILDINTERPRETEN, 2003: Luftbildinterpretationsschlüssel – Bestimmungsschlüssel für die Beschreibung von strukturreichen Waldbeständen im Color-Infrarot-Luftbild. Edited by Troyke, A., Habermann, R., Wolff, B., Gärtner, M., Engels, F., Brockamp, U., Hoffmann, K. et al. Pirna: Landesforstpräsidium (LFP) Freistaat Sachsen, 48.

AHRENS, W., BROCKAMP, U. & PISOKE, T., 2004: Zur Erfassung von Waldstrukturen im Luftbild. Arbeitsanleitung für Waldschutzgebiete Baden-Württemberg. Waldschutzgebiete Baden-Württemberg, **5**, 54.

BALASSO, M., 2016: Ecological requirements of the threetoed woodpecker (Picoides tridactylus L.) in boreal forests of northern Sweden, Master Thesis, Swedish University of Agricultural Sciences, https://stud.epsilon.slu.se/8777/, letzter Zugriff 03.02.24.

BAUHUS, J. & HERRMANN. S., 2010: Totholz - Bedeutung, Situation, Dynamik. 5. Wald-und-Klima.net.

BOUVET, A., PAILLET, Y. , ARCHAUX, F. , TILLON, L., DENIS, P., GILG O. & GOSSELIN, F., 2016: Effects of forest structure,management and landscape on bird and bat communities. Environ. Conservation, **43**(2), 148-160. https://doi.org/10.1017/S0376892915000363.

BRAUNISCH, V., 2008: Spatially explicit species-habitat models for large-scale conservation planning. Modelling habitat potential and habitat connectivity for capercaillie (Tetrao urogallus). Doctoral Thesis, Albert-Ludwigs-Universität Freiburg, 245 p.

ESA, EUROPEAN SPACE AGENCY, 2020: Sentinel 2. © ESA 2000 - 2020, Accessed 02.07.2020. https://sentinel.esa.int/web/sentinel/missions/sentinel-2.

EUROPEAN-SPACE-IMAGING, 2018: WorldView-3. Data Sheet. Munich. European Space Imaging.

FASSNACHT, F. E., 2013: Assessing the potential of imaging spectroscopy data to map tree species composition and bark beetle-related tree mortality. Doctoral Thesis, Faculty of Environment and Natural Resources, Albert-Ludwigs-University Freiburg, 99 p. https://freidok.uni-freiburg.de/data/9361, letzter Zugriff 03.02.24.

FASSNACHT, F. E., LATIFI, H., GOSH, A., JOSHI, P. K. & KOCH, B., 2014: Assessing the potential of hyperspectral imagery to map bark beetle-induced tree mortality. Remote Sensing of Environment, **140**, 533-48, https://doi.org/10.1016/j.rse.2013.09.014.

FASSNACHT, F., WHITE, J., WULDER, M. & NÆSSET, E., 2023: Remote sensing in forestry: current challenges, considerations and directions. Forestry: An International Journal of Forest Research, https://doi.org/10.1093/forestry/cpad024.

GANZ, S., KÄBER, Y. & ADLER, P., 2019: Measuring Tree Height with Remote Sensing - A Comparison of Photogrammetric and LiDAR Data with Different Field Measurements. Forests, **10**(694),14, https://doi.org/10.3390/f10080694.

HELL, M., BRANDMEIER, M., BRIECHLE, S. & KRZYSTEK, P., 2022: Classification of Tree Species and Standing Dead Trees with Lidar Point Clouds Using Two Deep Neural Networks: PointCNN and 3DmFV-Net. PFG – Journal of Photogrammetry, Remote Sensing and Geoinformation Science, **90**, 103-121, https://doi.org/10.1007/s41064-022-00200-4.

HENDEL, A.-L., WINIGER, N., JONKER, M., ZIELEWSKA-BÜTTNER, K., GANZ, S., ADLER, P. & BRAUNISCH, V., 2023: Bat habitat selection reveals positive effects of retention forestry. Forest Ecology and Management, **531**, 120783. https://doi.org/10.1016/j.foreco.2023.120783.

HEURICH, M., KRZYSTEK, P., POLAKOWSKY, F., LATIFI, H., KRAUSS, A. & MÜLLER, J., 2015: Erste Waldinventur auf Basis von Lidardaten und digitalen Luftbildern im Nationalpark Bayerischer Wald. Forstliche Forschungsberichte München, **214**, 101-113.

HIJMANS, J. R., 2020: raster: Geographic Data Analysis and Modeling. R package version 3.0-12.

HILDEBRANDT, G., 1996: Fernerkundung und Luftbildmessung für Forstwirtschaft, Vegetationskartierung und Landschaftsökologie. Heidelberg: Wichmann Verlag.

JUTRAS-PERREAULT, M.-C., GOBAKKEN, T., NÆSSET, E. & ØRKA, H. O., 2023: Comparison of Different Remotely Sensed Data Sources for Detection of Presence of Standing Dead Trees Using a Tree-Based Approach. Remote Sensing, **15**(9), https://doi.org/10.3390/rs15092223.

KAMIŃSKA, A., LISIEWICZ, M., KRASZEWSKI, B. & STEREŃCZAK, K., 2020: Habitat and stand factors related to spatial dynamics of Norway spruce dieback driven by Ips typographus (L.) in the Białowieża Forest District. Forest Ecology and Management, **476**, 118432, https://doi.org/10.1016/j.foreco.2020.118432.

KAMIŃSKA, A., LISIEWICZ, M., STEREŃCZAK, K., KRASZEWSKI, B. & SADKOWSKI, R., 2018: Species-related single dead tree detection using multi-temporal ALS data and CIR imagery. Remote Sensing of Environment, **219**, 31-43. https://doi.org/10.1016/j.rse.2018.10.005.

KEBRLE, D., ZASADIL, P., BARTÁK, V. & HOFMEISTER, J., 2022: Bird response to forest disturbance size in mountain spruce forests in Central Europe. Forest Ecology and Management, **524**, 120527. https://doi.org/10.1016/j.foreco.2022.120527.

KORTMANN, M., HURST, J., BRINKMANN, R., HEURICH, M., SILVEYRA GONZÁLEZ, R., MÜLLER, J. & THORN, S., 2018: Beauty and the beast: how a bat utilizes forests shaped by outbreaks of an insect pest. Animal Conservation, **21**(1), 21-30. https://doi.org/10.1111/acv.12359.

KRZYSTEK, P., SEREBRYANYK, A., SCHNÖRR, C., ČERVENKA, J. & HEURICH, M., 2020: Large-Scale Mapping of Tree Species and Dead Trees in Šumava National Park and Bavarian Forest National Park Using Lidar and Multispectral Imagery. Remote Sensing, **12**(4), 661, https://doi.org/10.3390/rs12040661.

KUHN, M., WING, J., WESTON, S., WILLIAMS, A., KEEFER, C., ENGELHARDT, A., COOPER, T., MAYER, Z., KENKEL, B., R CORE TEAM, BENESTY, M., LESCARBEAU, R., ZIEM, A., SCRUCCA, L., TANG, Y., CANDAN, C. & HUNT, T., 2023: Package 'caret'. Classification and Regression Training. Edited by Kuhn, M., Misc functions for training and plotting classification and regression models.

KUULUVAINEN, T., ANGELSTAM, P., FRELICH, L., JÕGISTE, K., KOIVULA, M., KUBOTA, Y., LAFLEUR, B. & MACDONALD, E., 2021: Natural Disturbance-Based Forest Management: Moving Beyond Retention and Continuous-Cover Forestry. Frontiers in Forests and Global Change, **4**, https://doi.org/10.3389/ffgc.2021.629020.

LASSAUCE, A., PAILLET, Y., JACTEL, H. & BOUGET, C., 2011: Deadwood as a surrogate for forest biodiversity: Meta-analysis of correlations between deadwood volume and species richness of saproxylic organisms. Ecological indicators, **11(5)**, 1027-39, https://doi.org/10.1016/j.ecolind.2011.02.004.

LGL, LANDESAMT FÜR GEOINFORMATION UND LANDENTWICKLUNG BADEN-WÜRTTEMBERG, 2022: Luftbildprodukte. https://www.lgl-bw.de/Produkte/Geodatendienste/Luftbildprodukte/, letzter Zugriff 03.02.24.

LGL, LANDESAMT FÜR GEOINFORMATION UND LANDENTWICKLUNG BADEN-WÜRTTEMBERG, 2023a: Bildbasiertes Digitales Oberflächenmodell (bDOM). https://www.lgl-bw.de/Produkte/3D-Produkte/Digitale-Oberflaechenmodelle/bDOM/, letzter Zugriff 03.02.24.

LGL, LANDESAMT FÜR GEOINFORMATION UND LANDENTWICKLUNG BADEN-WÜRTTEMBERG, 2023b: Digitale Geländemodelle (DGM). Accessed 2023.12.04. https://www.lgl-bw.de/Produkte/3D-Produkte/Digitale-Gelaendemodelle/, letzter Zugriff 03.02.24.

LIU, X., FREY, J., DENTER, M., ZIELEWSKA-BÜTTNER, K., STILL, N. & KOCH, B., 2021: Mapping standing dead trees in temperate montane forests using a pixel- and object-based image fusion method and stereo WorldView-3 imagery. Ecological indicators, **133**, 108438, https://doi.org/10.1016/j.ecolind.2021.108438.

MEDDENS, A. J. H., HICKE, J. A., & VIERLING, L. A., 2011: Evaluating the potential of multispectral imagery to map multiple stages of tree mortality. Remote Sensing of Environment, **115**(7), 1632-1642. https://doi.org/10.1016/j.rse.2011.02.018.

MÜLLER, J., NOSS, R. F., THORN, S., BÄSSLER, C., LEVERKUS, A. B. & LINDENMAYER, D. B., 2018: Increasing disturbance demands new policies to conserve intact forest. Conservation Letters, **e12449**, https://doi.org/10.1111/conl.12449.

NÄSI, R., HONKAVAARA, E., BLOMQVIST, M., LYYTIKÄINEN-SAARENMAA, P., HAKALA, T., VILJANEN, N., KANTOLA, T. & HOLOPAINEN, M., 2018: Remote sensing of bark beetle damage in urban forests at individual tree level using a novel hyperspectral camera from UAV and aircraft. Urban Forestry & Urban Greening, **30**, 72-83. https://doi.org/10.1016/j.ufug.2018.01.010.

NFRAMES_GMBH, (2024): "nFRAMES." https://www.nframes.com/, letzter Zugriff 20.01.24.

NOWAKOWSKA, J.A., HSIANG, T., PATYNEK, P., STEREŃCZAK, K., OLEJARSKI, I. & OSZAKO, T., 2020: Health Assessment and Genetic Structure of Monumental Norway Spruce Trees during A Bark Beetle (Ips typographus L.) Outbreak in the Białowieża Forest District, Poland. Forests, **11**(647), https://doi.org/10.3390/f11060647.

PLUTO-KOSSAKOWSKA, J., OSINSKA-SKOTAK, K. & STEREŃCZAK, K., 2017: Determining the spatial resolution of multispectral satellite images optimal to detect dead trees in forest areas. Sylwan, **161**(5), 395-404.

RAKOVEC, O., SAMANIEGO, L., HARI, V., MARKONIS, Y., MORAVEC, V., THOBER, S., HANEL, M. & KUMAR, R., 2022: The 2018-2020 Multi-Year Drought Sets a New Benchmark in Europe. Earth's Future, **10**(3), e2021EF002394, https://doi.org/10.1029/2021EF002394.

RAPIDLASSO GMBH, 2022: LAStools - efficient LiDAR processing software (version 221111). http://rapidlasso.com/LAStools, letzter Zugriff 03.02.24.

R CORE TEAM, 2023: R: A language and environment for statistical computing. The R Foundation for Statistical Computing

RSTUDIO, 2023: RStudio: Integrated Development for R. "Mountain Hydrangea" Release. © 2009-2023 Posit Software, PBC.

SCHIEFER, F., SCHMIDTLEIN, S., FRICK, A., FREY, J., KLINKE, R., ZIELEWSKA-BÜTTNER, K., JUNTTILA, S., UHL, A. & KATTENBORN, T., 2023: UAV-based reference data for the prediction of fractional cover of standing deadwood from Sentinel time series. ISPRS Open Journal of Photogrammetry and Remote Sensing **8**, 100034, https://doi.org/10.1016/j.ophoto.2023.100034.

SCHULDT, B., BURAS, A., AREND, M., VITASSE, Y., BEIERKUHNLEIN, C., DAMM, A., GHARUN, M. et al., 2020: A first assessment of the impact of the extreme 2018 summer drought on Central European forests. Basic and Applied Ecology, **45**, 86-103, https://doi.org/10.1016/j.baae.2020.04.003.

SCHUMACHER, J., RATTAY, M., KIRCHHÖFER, M., ADLER, P. & KÄNDLER, G., 2019: Combination of Multi-Temporal Sentinel Images Aerial Image Based Canopy Height Models for Timber Volume Modelling. Forests, **10**(9), 746, https://doi.org/10.3390/f10090746.

SCHWARZ, S., WERNER, C., FASSNACHT, F. E. & RUEHR, N. K., 2023: Forest canopy mortality during the 2018-2020 summer drought years in Central Europe: The application of a deep learning approach on aerial images across Luxembourg. Forestry: An International Journal of Forest Research, **cpad049**. https://doi.org/10.1093/forestry/cpad049.

SEIBOLD, S., BRANDL, R., BUSE, J., HOTHORN, T., SCHMIDL, J., THORN, S. & MÜLLER, J., 20165: Association of extinction risk of saproxylic beetles with ecological degradation of forests in Europe. Conserv Biology, **29**, 382-390. https://doi.org/10.1111/cobi.12427.

SEIDL, R., MÜLLER, J., HOTHORN, T., BÄSSLER, C., HEURICH, M. & KAUTZ, M., 2016: Small beetle, large-scale drivers: how regional and landscape factors affect outbreaks of the European spruce bark beetle. Journal of Applied Ecology, **53**, 530-40, https://doi.org/10.1111/1365-2664.12540.

SENF, C., & SEIDL, R., 2018: Natural disturbances are spatially diverse but temporally synchronized across temperate forest landscapes in Europe. Glob Change Biology, **24**, 1201-1211, https://doi.org/10.1111/gcb.13897.

SENF, C., & SEIDL, R., 2021: Persistent impacts of the 2018 drought on forest disturbance regimes in Europe. Biogeosciences, **18**, 5223-5230. https://doi.org/10.5194/bg-18-5223-2021.

SPIECKER, H. & KAHLE. H.-P., 2023: Climate-driven tree growth and mortality in the Black Forest, Germany - Long-term observations. Global Change Biology, **29**(20), 5908-5923, https://doi.org/10.1111/gcb.16897.

STEREŃCZAK, K., KRASZEWSKI, B., MIELCAREK, M. & PIASECKA, Z., 2017: Inventory of standing dead trees in the surroundings of communication routes – The contribution of remote sensing to potential risk assessments. Forest Ecology and Management, **402**, 76-91, https://doi.org/10.1016/j.foreco.2017.07.018.

STIGHÄLL, K., ROBERGE, J.-M., ANDERSSON, K. & ANGELSTAM, P., 2011: Usefulness of biophysical proxy data for modelling habitat of an endangered forest species: The white-backed woodpecker Dendrocopos leucotos. Scandinavian Journal of Forest Research, **26**(6), 576-85, https://doi.org/10.1080/02827581.2011.599813.

THOM, D. & KEETON, W. S., 2020: Disturbance-based silviculture for habitat diversification: Effects on forest structure, dynamics, and carbon storage. Forest Ecology and Management, **469**, 118132, https://doi.org/10.1016/j.foreco.2020.118132.

THORN, S., BÄSSLER, C., SVOBODA, M. & MÜLLER, J., 2017: Effects of natural disturbances and salvage logging on biodiversity – Lessons from the Bohemian Forest. Forest Ecology and Management, **388**, 113-119, https://doi.org/10.1016/j.foreco.2016.06.006.

VÍTKOVÁ, L., BAČE, R., KJUČUKOV, P. & SVOBODA, M., 2018: Deadwood management in Central European forests: Key considerations for practical implementation. Forest Ecology and Management, **429**, 394-405, https://doi.org/10.1016/j.foreco.2018.07.034.

WHITE, J., COOPS, N. C., WULDER, M. A., VASTARANTA, M., HILKER, T. & TOMPALSKI, P., 2016: Remote Sensing Technologies for Enhancing Forest Inventories: A Review. Canadian Journal of Remote Sensing, **42**(5), 619-641, https://doi.org/10.1080/07038992.2016.1207484.

WHITE, J., TOMPALSKI, P., COOPS, N. & WULDER, M., 2018: Comparison of airborne laser scanning and digital stereo imagery for characterizing forest canopy gaps in coastal temperate rainforests. Remote Sensing of Environment, **208**, 1-14, https://doi.org/10.1016/j.rse.2018.02.002.

ZIELEWSKA-BÜTTNER, K., 2020: Deriving biodiversity-relevant forest structure parameters: The value of aerial imagery from state surveys. Doctoral Thesis, Albert-Ludwigs Universität, 163, https://freidok.uni-freiburg.de/data/193860, letzter Zugriff 03.20.24.

ZIELEWSKA-BÜTTNER, K., ADLER, P., KOLBE, S., BECK, R., GANTER, L. M., KOCH, B. & BRAUNISCH, V., 2020: Detection of Standing Deadwood from Aerial Imagery Products: Two Methods for Addressing the Bare Ground Misclassification Issue. Forests, **11**(8), https://doi.org/10.3390/f11080801.

ZIELEWSKA-BÜTTNER, K., ADLER, P., PETERESEN, M. & BRAUNISCH, V., 2016: Parameters Influencing Forest Gap Detection Using Canopy Height Models Derived From Stereo Aerial Imagery. Paper presented at the 3. Wissenschaftlich-Technische Jahrestagung der DGPF. Dreiländertagung der DGPF, der OVG und der SGPF, Bern, Schweiz. https://www.dgpf.de/src/tagung/jt2016/proceedings/papers/38_DLT2016_Zielewska-Buettner_et_al.pdf.

ZIELEWSKA-BÜTTNER, K., HEURICH, M., MÜLLER, J. & BRAUNISCH, V., 2018: Remotely Sensed Single Tree Data Enable the Determination of Habitat Thresholds for the Three-Toed Woodpecker (Picoides tridactylus). Remote Sensing, **10**(1972), 1-25, https://doi.org/10.3390/rs10121972.

7 Supplementary material

Appendix 1: Distribution of the validation pixels different model classes: bare ground, live, declining and dead in the study area presented on the background color-infrared (CIR) orthophoto.

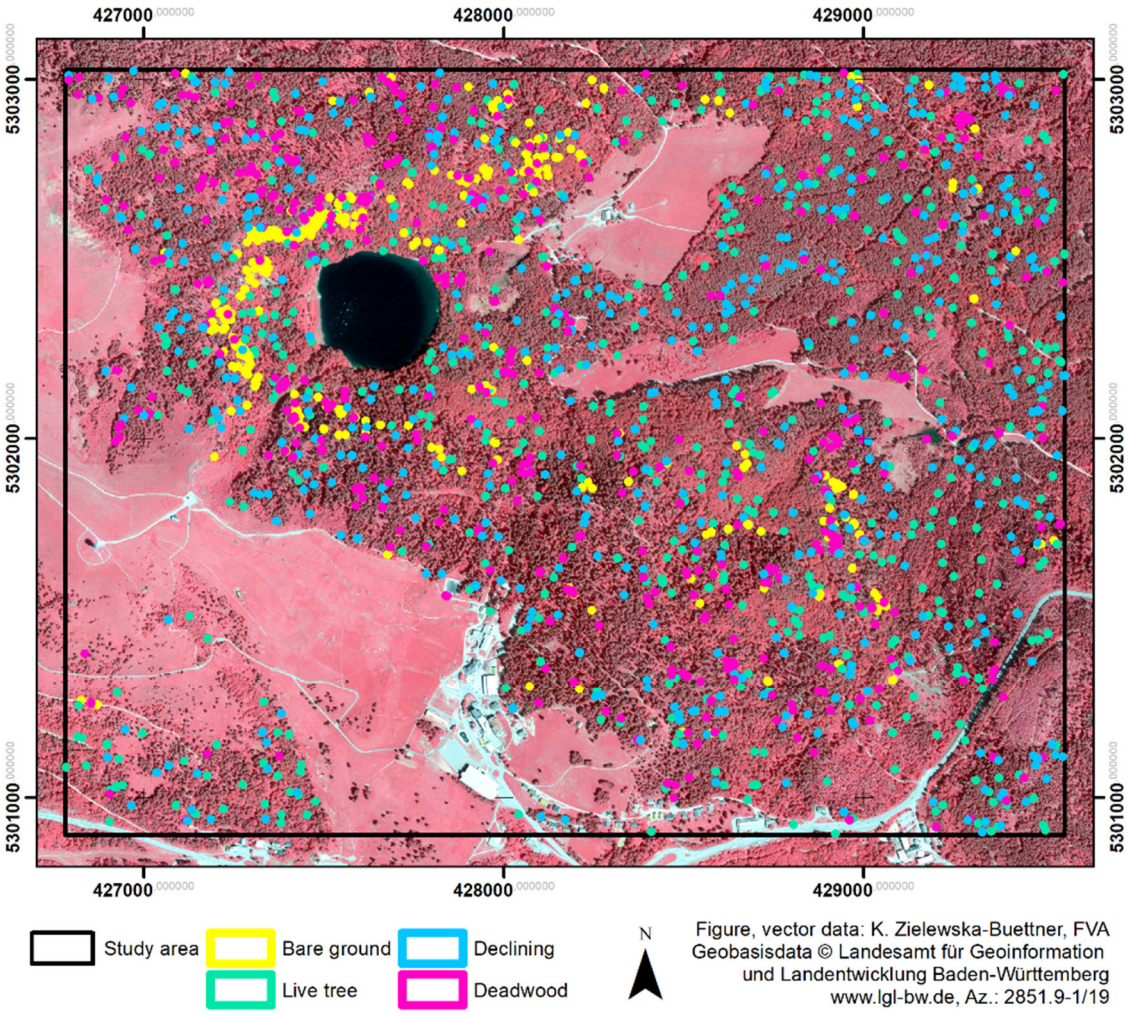

Appendix 2 Six confusion matrix illustrating results of visual validation per model class against results of RF deadwood mapping based on six predefined test datasets of different orthophoto resolution and alternating VHM settings. Datasets are specified in Table 2. Visual validation was extended by additional classes: building, orthophoto artefact and shadow.

Test data-set	Data type	Visual validation								
		Class	Bare ground	Live	Decli-ning	Dead	Buil-ding	Ortho-photo ar-tefact	Sha-dow	Sum
2019_02_1H	Prediction	Bare ground	239	1	54	42	0	0	0	336
		Live	1	458	36	0	0	0	0	495
		Declining	15	28	477	14	0	0	0	534
		Dead	82	2	56	394	6	0	0	540
		Sum	337	489	623	450	6	0	0	1905
2019_02_1L	Prediction	Bare ground	162	2	51	45	0	12	9	281
		Live	0	426	40	0	0	0	16	482
		Declining	12	25	442	15	0	1	16	511
		Dead	68	0	29	318	4	3	5	427
		Sum	242	453	562	378	4	16	46	1701
2019_02_05H	Prediction	Bare ground	251	1	69	44	0	23	21	409
		Live	0	457	36	0	0	0	19	512
		Declining	14	29	474	10	0	0	5	532
		Dead	75	2	46	396	6	2	15	542
		Sum	340	489	625	450	6	25	60	1995
2019_02_05L	Prediction	Bare ground	214	2	58	46	0	19	17	356
		Live	0	453	34	0	0	0	17	504
		Declining	19	28	480	13	0	0	14	554
		Dead	70	0	37	380	5	3	9	504
		Sum	303	483	609	439	5	22	57	1918
2019_05_05H	Prediction	Bare ground	198	0	51	23	0	0	0	272
		Live	3	464	59	0	0	0	0	526
		Declining	18	45	413	12	0	0	0	488
		Dead	89	2	52	361	6	0	0	510
		Sum	308	511	575	396	6	0	0	1796
2019_05_05L	Prediction	Bare ground	202	0	56	34	0	0	0	292
		Live	0	473	45	0	0	0	0	518
		Declining	4	30	421	7	0	0	0	462
		Dead	75	2	39	343	6	0	0	465
		Sum	281	505	561	384	6	0	0	1737

Appendix 3: Six confusion matrix illustrating results of visual validation per model class against results of the deadwood mapping final stage UNC based on six predefined test datasets of different orthophoto resolution and alternating VHM settings. Datasets are specified in Table 2. Visual validation was extended by additional classes: building, orthophoto artefact and shadow.

Test data-set	Data type	Visual validation								
		Class	Bare ground	Live	Declining	Dead	Building	Orthophoto artefact	Shadow	Sum
2019_02_1H	Prediction	Bare ground	240	1	58	43	0	21	16	379
		Live	1	458	36	0	0	0	20	515
		Declining	15	28	477	14	0	0	12	546
		Dead	81	2	52	393	6	4	12	550
		Sum	337	489	623	450	6	25	60	1990
2019_02_1L	Prediction	Bare ground	253	2	73	46	0	23	24	421
		Live	0	457	36	0	0	0	19	512
		Declining	14	29	474	10	0	0	5	532
		Dead	73	1	42	394	6	2	12	530
		Sum	340	489	625	450	6	25	60	1995
2019_02_05H	Prediction	Bare ground	165	2	52	45	0	12	9	285
		Live	0	426	40	0	0	0	16	482
		Declining	12	25	442	15	0	1	16	511
		Dead	65	0	28	318	4	3	5	423
		Sum	242	453	562	378	4	16	46	1701
2019_02_05L	Prediction	Bare ground	217	2	61	47	0	19	19	365
		Live	0	453	34	0	0	0	17	504
		Declining	19	28	480	13	0	0	14	554
		Dead	67	0	34	379	5	3	7	495
		Sum	303	483	609	439	5	22	57	1918
2019_05_05H	Prediction	Bare ground	235	0	78	32	0	0	0	345
		Live	3	464	59	0	0	0	0	526
		Declining	18	45	413	12	0	0	0	488
		Dead	52	2	25	352	6	0	0	437
		Sum	308	511	575	396	6	0	0	1796
2019_05_05L	Prediction	Bare ground	229	0	84	37	0	0	0	350
		Live	0	473	45	0	0	0	0	518
		Declining	4	30	421	7	0	0	0	462
		Dead	48	2	11	340	0	0	0	401
		Sum	281	505	561	384	0	0	0	1731

Appendix 4: Maps showing classification results for six test datasets with different orthophoto and Vegetation Height Models setting at two-stages of the mapping algorithm: Random Forest Model and Uncertainty Model. Datasets are specified in Table 2. RGB and CIR orthophotos are presented for reference

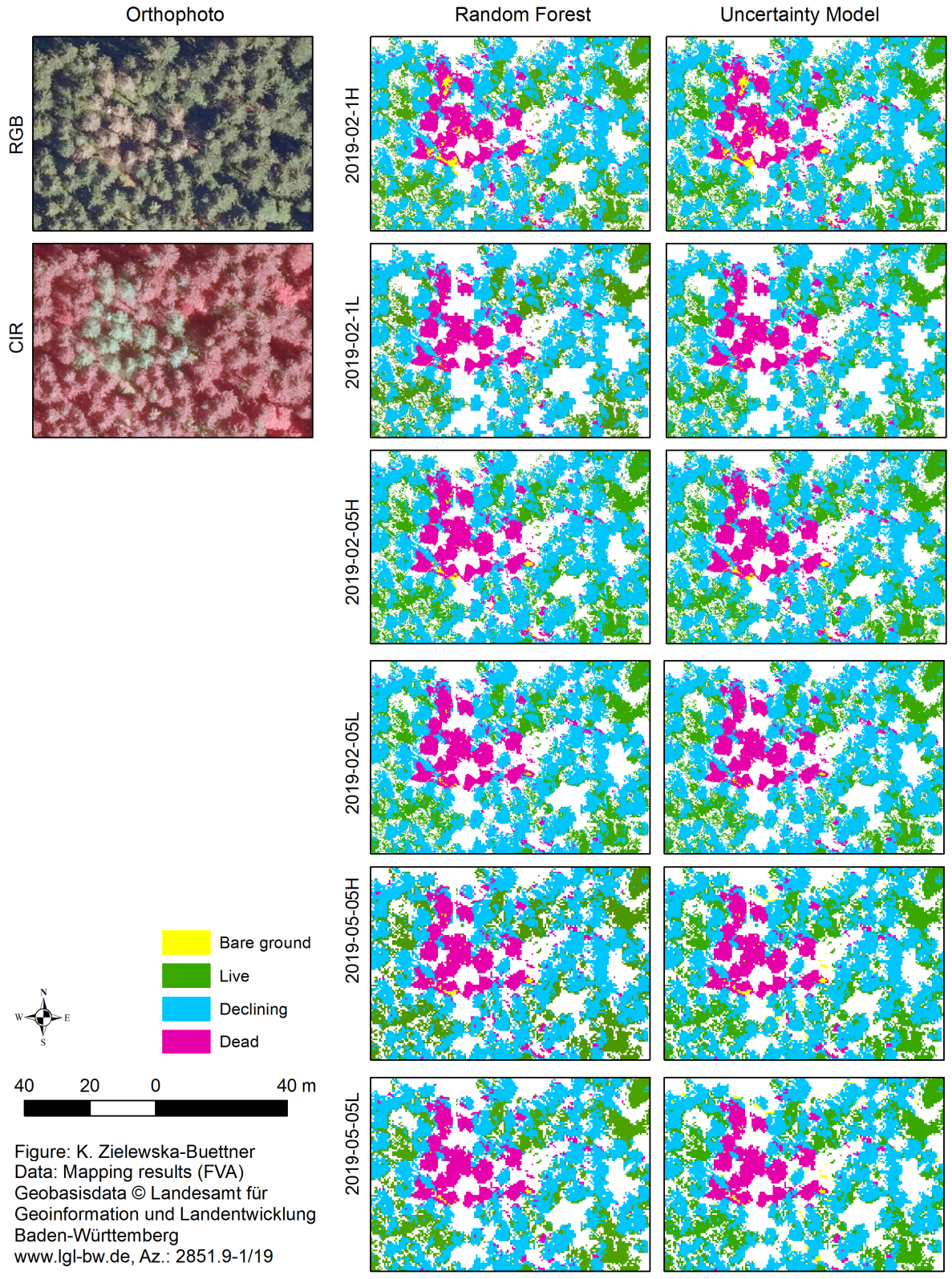

Figure: K. Zielewska-Buettner
Data: Mapping results (FVA)
Geobasisdata © Landesamt für Geoinformation und Landentwicklung Baden-Württemberg
www.lgl-bw.de, Az.: 2851.9-1/19